A dual function of Bcl11b/Ctip2 in hippocampal neurogenesis

Ruth Simon[1,8], Heike Brylka[1,2,3,8],
Herbert Schwegler[4],
Sathish Venkataramanappa[1],
Jacqueline Andratschke[1],
Christoph Wiegreffe[1], Pentao Liu[5],
Elaine Fuchs[6], Nancy A Jenkins[7],
Neal G Copeland[7], Carmen Birchmeier[3]
and Stefan Britsch[1,2,3,*]

[1]Institute of Molecular and Cellular Anatomy, Ulm University, Ulm, Germany, [2]Center for Anatomy, Georg-August-University, Goettingen, Germany, [3]Max Delbrück Center for Molecular Medicine (MDC), Berlin-Buch, Germany, [4]Institute of Anatomy, Otto-von-Guericke University, Magdeburg, Germany, [5]The Wellcome Trust Sanger Institute, Cambridge, UK, [6]HHMI, Rockefeller University, New York, NY, USA and [7]Cancer Research Program, The Methodist Hospital Research Institute, Houston, TX, USA

The development of the dentate gyrus is characterized by distinct phases establishing a durable stem-cell pool required for postnatal and adult neurogenesis. Here, we report that *Bcl11b/Ctip2*, a zinc finger transcription factor expressed in postmitotic neurons, plays a critical role during postnatal development of the dentate gyrus. Forebrain-specific ablation of *Bcl11b* uncovers dual phase-specific functions of *Bcl11b* demonstrated by feedback control of the progenitor cell compartment as well as regulation of granule cell differentiation, leading to impaired spatial learning and memory in mutants. Surprisingly, we identified Desmoplakin as a direct transcriptional target of *Bcl11b*. Similarly to *Bcl11b*, postnatal neurogenesis and granule cell differentiation are impaired in Desmoplakin mutants. Re-expression of Desmoplakin in *Bcl11b* mutants rescues impaired neurogenesis, suggesting Desmoplakin to be an essential downstream effector of *Bcl11b* in hippocampal development. Together, our data define an important novel regulatory pathway in hippocampal development, by linking transcriptional functions of *Bcl11b* to Desmoplakin, a molecule known to act on cell adhesion.

*Corresponding author. Institute of Molecular and Cellular Anatomy, Ulm University, Albert-Einstein-Allee 11, Ulm 89081, Germany. Tel.: +49 731 500 23101; Fax: +49 731 500 23102; E-mail: stefan.britsch@uni-ulm.de
[8]These authors contributed equally to this work

Introduction

Hippocampal structures play an important role in memory and learning as well as in emotional behaviour. The dentate gyrus, the primary gateway for input information into the hippocampus, is one of only two brain regions with continuous neurogenesis in adult mammals. Development and postnatal function of the dentate gyrus are characterized by distinct phases involving specific molecular pathways (Kempermann *et al*, 2004; Frotscher *et al*, 2007; Li and Pleasure, 2007). While dentate gyrus morphogenesis starts early in embryonic development, the vast majority of neurons are born within the first 4 postnatal weeks (Muramatsu *et al*, 2007). During this time, the proliferative compartment becomes restricted to the subgranular zone (SGZ) positioned between hilus and granule cell layer (GCL) providing the stem-cell pool for continuous neurogenesis throughout adulthood (Altman and Bayer, 1990). The progression from stem/progenitor cell to mature neuron requires several steps, including migration and positioning of the newborn cells, growth and target finding of axons and dendrites of the immature neuron, and finally the synaptic integration of the mature neuron. Several transcription factors and signalling pathways, most of them commonly used in cellular differentiation, are required for the development of the hippocampus (Kempermann *et al*, 2004; Frotscher *et al*, 2007; Li and Pleasure, 2007). Previous work has demonstrated that both the transcription factors *NeuroD* and *Prox1* are regulated by β-catenin implying the involvement of the *Wnt* signalling pathway in the regulation of hippocampal granule cells (Liu *et al*, 2000; Pleasure *et al*, 2000; Gao *et al*, 2009; Kuwabara *et al*, 2009; Karalay *et al*, 2011). Transcription factors also play an important role in proliferation and maintenance of neural stem/precursor cells as was shown for *Sox2* (Ferri *et al*, 2004; Favaro *et al*, 2009). However, mechanisms underlying the phase-specific control of postnatal hippocampal development are still incompletely understood.

To further elucidate the mechanisms of postnatal neurogenesis of the dentate gyrus, we studied *Bcl11b*, a Krüppel-like C_2H_2 zinc finger transcription factor expressed in the hippocampus, neocortex (Arlotta *et al*, 2005; Chen *et al*, 2008; Seuntjens *et al*, 2009) and the striatum (Arlotta *et al*, 2008; Desplats *et al*, 2008). *Bcl11b* plays an important role in the prenatal development of corticospinal motor neurons as well as specific subsets of striatal neurons (Arlotta *et al*, 2005, 2008; Chen *et al*, 2008).

Here, we show a dual phase-specific function of *Bcl11b* restricted to postnatal development of the dentate gyrus. Our studies demonstrate that *Bcl11b*, expressed in postmitotic granule neurons, is involved in the regulation of progenitor proliferation by a feedback mechanism. As a consequence, proliferating progenitor cells are reduced, and postmitotic dentate granule cells are depleted in *Bcl11b* mutants. Moreover, the differentiation of postmitotic neurons depends

on *Bcl11b* expression, and mutant neurons fail to integrate into hippocampal circuitry leading to impaired learning and memory. We identified Desmoplakin as a direct target gene of *Bcl11b*. Forebrain-specific deletion of Desmoplakin results in developmental defects similar to those observed in *Bcl11b* mutants as demonstrated by reduced cell proliferation and impaired neuronal differentiation. Moreover, re-introduction of Desmoplakin into the *Bcl11b* mutant dentate gyrus rescues the deficit in neurogenesis. Thus, our data define important functions of *Bcl11b* in postnatal hippocampal development. Furthermore, we identify Desmoplakin to be a critical downstream effector of *Bcl11b* in regulating hippocampal neurogenesis.

Results

Analysis of Bcl11b expression in the hippocampus

Bcl11b expression was first observed at embryonic stage 15 (E15), restricted to the Cornu Ammonis (CA) and expanding to the suprapyramidal blade of the developing dentate gyrus at E18 (Supplementary Figure S1A–D). During postnatal development, *Bcl11b* is expressed in dentate granule cells and in the CA1 and CA2 regions (Supplementary Figure S1 E–H). *NeuroD*, a transcription factor expressed by newborn, migrating as well as early differentiating, neurons (Pleasure *et al*, 2000), colocalizes with all *Bcl11b* expressing cells in the prospective suprapyramidal blade at E18 but not in cells migrating into the dentate primordium (Figure 1A and D). Postnatal dentate development results in a gradient of granule cell differentiation with newborn progenitor cells located in the SGZ and mature granule cells in the most superficial zone of the GCL (Figure 1). Expression analysis of *NeuroD* at P7 identified a cluster of cells co-expressing *Bcl11b* located in the middle of the GCL but no *Bcl11b* co-expressing cells were found in the SGZ (Figure 1B and E). Only a few cells residing in the outer layer of the GCL were co-expressing *Bcl11b* and the postmitotic marker genes, *NeuN* and Calbindin (*Calb1*) at P7 (Figure 1H and I). At P30, strong expression of *NeuroD* is limited to the innermost GCL and the SGZ with only very few cells co-expressing *Bcl11b* (Figure 1C and F). Similar results were obtained for Doublecortin (*Dcx*), expressed in both progenitor cells and immature neurons (Kempermann *et al*, 2004; Figure 1G and J). At this stage, the majority of *Bcl11b*-positive cells located in all parts of the GCL are co-expressing *NeuN* and *Calb1* (Figure 1K and L). Together, this suggests that *Bcl11b* expression is restricted to postmitotic granule neurons of the dentate gyrus but excluded from proliferating progenitor cells. This is confirmed by the mutually exclusive expression of *Bcl11b* and *Sox2*, expressed in stage 1 stem cells and *Tbr2*, a marker for stage 2 and 3 progenitor cells (Ferri *et al*, 2004; Hodge *et al*, 2008; Figure 1M–O).

Development of the dentate gyrus requires Bcl11b expression

To determine the functions of *Bcl11b* in the developing dentate gyrus, we generated conditional knock-out mice by mating *Bcl11b*^flox/flox^ mice (Li *et al*, 2010) with the forebrain-specific Emx1-*Cre* mouse line (Gorski *et al*, 2002). Expression of Emx1-*Cre* occurs in mitotic as well as in postmitotic cells of the telencephalon early on in development (Gorski *et al*, 2002; Supplementary Figure S2A and B). Homozygous *Bcl11b*^flox/flox^;Emx1-*Cre* offspring exhibit complete ablation

of *Bcl11b* protein in the hippocampus (Supplementary Figure S2C and D). Histological analysis of *Bcl11b* mutants revealed no change in the overall architecture of the hippocampus but a reduction in size of the dentate gyrus as early as P7 as determined by analysis of dentate gyrus area and cell number (Supplementary Figure S3C–H). This size reduction is even more prominent at P30 especially in the infrapyramidal blade (Figure 2A–D). At this stage, the area of the dentate gyrus of mutant animals is 40% smaller (Figure 2E; $P < 0.005$) and the cell number is reduced by 33% (Figure 2F; $P < 0.05$) when compared with control animals. Examining embryonic stages did not show any obvious differences between control and mutant animals (Supplementary Figure S3A and B), which might be due to the restricted expression of *Bcl11b* in the hippocampus during prenatal development. In addition to the reduced cell number, the mutant dentate gyrus exhibits granule cell dispersion; granule cells of control animals are densely packed in a distinct layer while in the mutant these cells are loosely organized (Figure 2C and D; Supplementary Figure S3G and H). Furthermore, cells with abnormal morphology were increased, their nuclei appeared smaller and stained darker when compared with control cells, representing most likely immature precursor-like cells.

Loss of Bcl11b reduces neuronal progenitor cell proliferation

The loss of dentate granule cells in *Bcl11b* mutants might be either due to reduced cell survival or proliferation. TUNEL analysis at P14 revealed a total increase of apoptotic cells in the mutant dentate gyrus (Figure 3A–C; control: 2.9 ± 0.34 s.e.m.; mutant: 12.94 ± 1.55 s.e.m.; $P < 0.05$). Examining the distribution of apoptotic cells demonstrated significantly increased numbers in the GCL (control: GCL, 52.4%; mutant: 64.3%; $P < 0.05$) but no change in the SGZ of mutants (Figure 3C). To identify proliferating cells within the dentate gyrus, we performed short-pulse labelling with BrdU. At E18, *Bcl11b* mutant and control animals do not exhibit differences in proliferation within the dentate gyrus anlage (Supplementary Figure S4A–C). Examining proliferating cells of the postnatal dentate gyrus revealed a greatly reduced number of BrdU-positive cells at P7 (25% fewer BrdU-positive cells, $P < 0.05$; Supplementary Figure S4D–F) and at P14 when the majority of proliferating progenitor cells are located in the newly developed SGZ (25% fewer BrdU-positive cells, $P < 0.0005$; Figure 3D, E and K). This proliferation deficit was confined to the SGZ (44% reduction, $P < 0.0005$; Figure 3K), while no changes in the number of BrdU-positive cells were detected in the GCL of Bcl11b mutants (Figure 3K). To further explore whether reduced proliferation was caused by a depletion of the dentate progenitor cell pool within the SGZ, we analysed numbers and distribution of *Sox2*-positive progenitor cells. Interestingly, while the overall numbers of *Sox2* expressing progenitors were unchanged we observed a significant depletion of *Sox2*-positive cells in the SGZ (60.6% of control; $P < 0.05$) with a shift of *Sox2* expressing cells to the GCL of *Bcl11b* mutants (157% of control, $P < 0.05$; Figure 3M). A similar depletion of progenitor cells specifically in the SGZ was observed when we used *Tbr2* as a progenitor marker (24.25% of control, $P < 0.05$; Figure 3O). Analysing BrdU incorporation by *Sox2* and *Tbr2* expressing cells, we found reduced numbers of BrdU-positive progenitor cells specifically in the SGZ (Figure 3I, J and O; *Sox2*/BrdU,
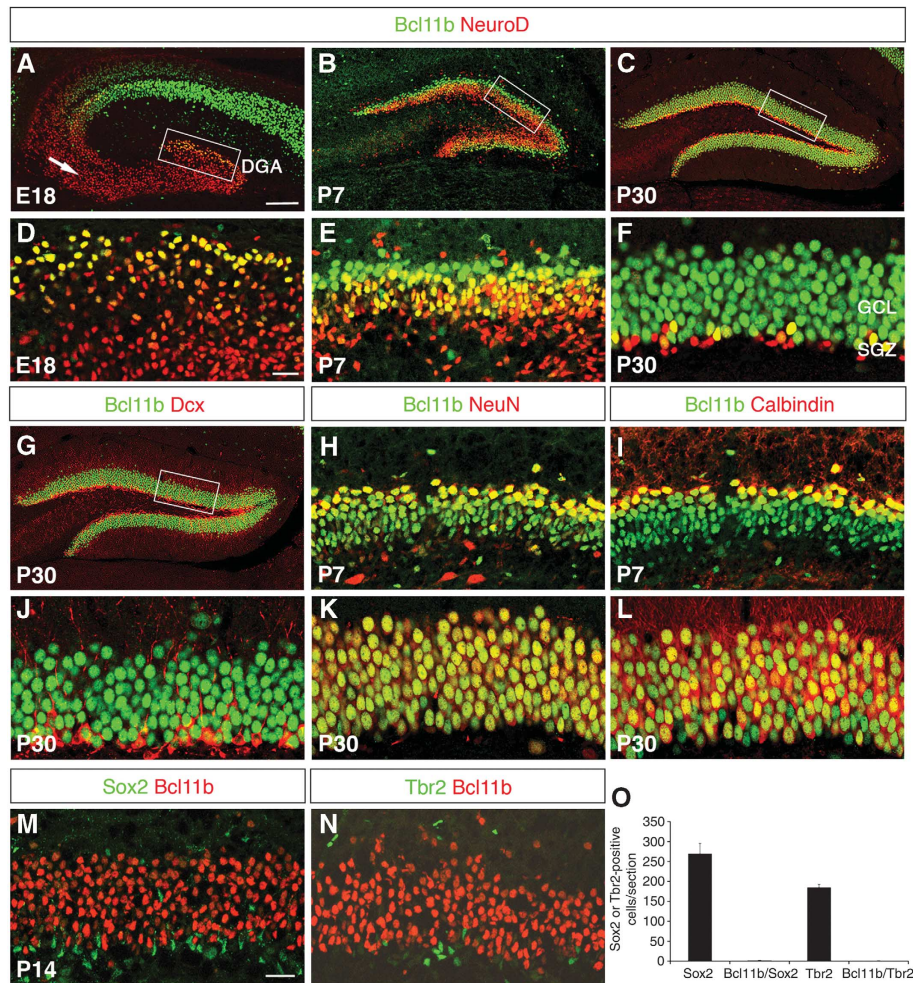
Figure 1 *Bcl11b* expression is restricted to postmitotic neurons during prenatal- and postnatal development of the hippocampus. (**A–L**) Immunohistological analysis of co-expression of *Bcl11b* (green) and *NeuroD* (red) at embryonic stage E18 (**A**, **D**) and postnatal stages P7 (**B**, **E**) and P30 (**C**, **F**); Doublecortin (*Dcx*; red) at P30 (**G**, **J**); *NeuN* (red) at P7 (**H**) and P30 (**K**); Calbindin (red) at P7 (**I**) and P30 (**L**). (**M**, **N**) Co-expression analysis of *Bcl11b* (red) and *Sox2* (**M**, green) as well as *Bcl11b* (red) and *Tbr2* (**N**, green) at P14. (**O**) Statistical analysis of **M** and **N**; no co-expression of *Bcl11b* with *Sox2* and *Tbr2* was detected (error bar, s.d.; $n = 3$). Confocal images taken at $\times 20$ (**A–C**, **G**) and $\times 63$ (**D–F**, **H–N**) magnification. Scale bar: 100 μm (**A**), 20 μm (**D**) and 25 μm (**M**). Rectangular box indicates area of higher magnification. Arrow indicates early migrating *NeuroD* expressing cells. DGA, dentate gyrus anlage; GCL, granule cell layer; SGZ, subgranular zone.

52.4% of control; *Tbr2*/BrdU, 44.4% of control; $P < 0.05$ for both). Together, our data suggest that reduced progenitor cell proliferation as observed specifically in the SGZ of the *Bcl11b* mutant dentate gyrus might be due to a depletion of the progenitor cell compartment. In mutants, part of the *Sox2*-positive cells are no longer confined to their natural positions within the SGZ and aberrantly distribute to the GCL where BrdU incorporation was found unchanged (Figure 3K and M). Thus, aberrantly localized progenitor cells may have lost part of their proliferation capacity.

Bcl11b expression is restricted to postmitotic granule cells (cf. Figure 1). Accordingly, at no time colocalization of *Bcl11b* and BrdU was observed (Figure 3F–H; Supplementary Figure S4G–L) posing the question whether *Bcl11b* regulates progenitor cells through indirect mechanisms. To further examine this, we generated *Bcl11b*[flox/flox];NexCre mice where Cre is almost exclusively restricted to postmitotic granule neurons (Goebbels *et al*, 2006; Seuntjens *et al*, 2009). Analysing these mice revealed a similar phenotype as observed in *Bcl11b*[flox/flox];Emx1-Cre mutants. At P14, *Bcl11b*[flox/flox];

NexCre hippocampi exhibit a reduced granule cell number (Supplementary Figure S5A–C; 83.8% of control, $P < 0.05$), increased apoptosis (Figure 3C; $P < 0.05$) as well as decreased BrdU incorporation specifically in the SGZ (Figure 3L; 44% (total) and 58% (SGZ) fewer BrdU-positive cells; $P < 0.05$). Similarly to *Bcl11b*[flox/flox];Emx1-*Cre* mutants, *Sox2*-positive cells were reduced in the SGZ and shifted to the GCL (Figure 3N; GCL: 145% of control; $P < 0.05$; SGZ: 72.8% of control; $0.1 \geqslant P \leqslant 0.05$) with *Sox2*/BrdU-positive cells specifically reduced in the SGZ of *Bcl11b*[flox/flox];NexCre mice (Figure 3O; 60.6% of control; $P < 0.05$). Collectively, these findings strongly suggest an indirect feedback mechanism for *Bcl11b* in the regulation of the progenitor compartment.

Bcl11b ablation impairs neuronal differentiation

To determine the role of *Bcl11b* in the regulation of granule cell differentiation, we examined the expression of stage-specific markers in control and *Bcl11b*[flox/flox];Emx1-*Cre* mutant animals. In controls, *Dcx* is localized in the cell body as well as in dendrites of cells of the innermost GCL
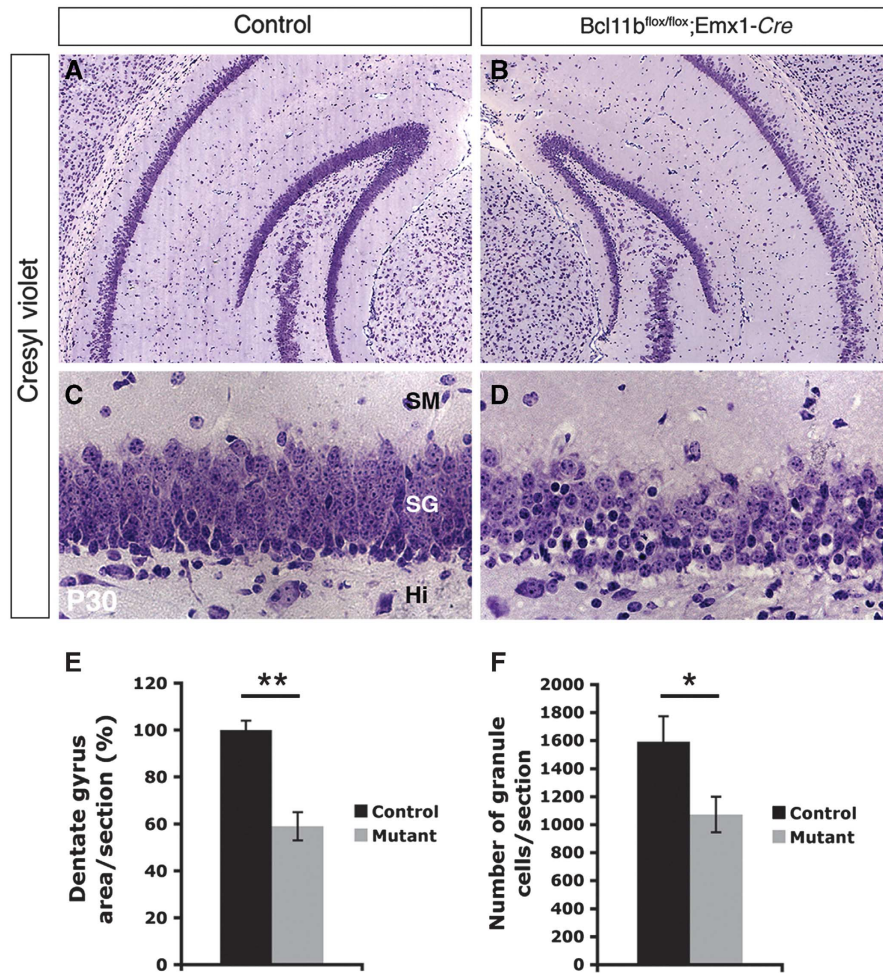
Figure 2 Ablation of *Bcl11b* expression causes morphological changes of the dentate gyrus. Representative coronal sections of control (**A**, **C**) and *Bcl11b*^flox/flox^;Emx-1*Cre* (**B**, **D**) animals at P30 stained with cresyl violet. Earlier developmental stages are presented in Supplementary Figure S3. Loss of *Bcl11b* expression causes reduced numbers of granule cells resulting in a smaller dentate gyrus. Statistical analysis of dentate gyrus area (**E**) and granule cell number (**F**) (*t*-test, *P<0.05; **P<0.005; error bars, s.e.m.; *n*=3). Brightfield images taken at ×5 (**A**, **B**) and ×63 (**C**, **D**) magnification. Hi, Hilus; SG, Stratum granulosum; SM, Stratum moleculare.

as well as the SGZ. Examining *Bcl11b*^flox/flox^;Emx1-*Cre* mutants at P30 revealed *Dcx*-positive cells distributed throughout the whole GCL (Figure 4A–D). In addition, while *Dcx*-expressing dendrites of control animals reach the outer surface of the molecular layer, *Dcx*-labelled mutant dendrites are much shorter ending in the inner molecular layer (Figure 4C and D). Moreover, we observed a two-fold increase of *NeuroD*-positive cells (Figure 4E–H; control 99.67 ± 9.34 s.e.m.; mutant 199.67 ± 7.92 s.e.m.; *t*-test, *P*<0.0005; *n*=3) in *Bcl11b* mutants. Similarly to *Dcx*, *NeuroD* expressing cells were no longer restricted to the innermost part of the GCL, suggesting that loss of *Bcl11b* expression impairs early neuronal differentiation, and immature neurons are no longer confined to their natural position within the dentate gyrus (Figure 4E–H). NeuN, expressed in immature as well as in mature granule neurons, and *Calb1*, expressed only in mature granule neurons, identify successive but overlapping stages of dentate granule cell differentiation (Kempermann *et al*, 2004). We observed strongly reduced *Calb1* expression starting as early as P7 (Figure 4I and J) accompanied by an increase of NeuN-

positive, *Calb1*-negative immature neurons in the dentate gyrus of *Bcl11b* mutants (Figure 4K–N). Together, this indicates that the differentiation of *Bcl11b* mutant dentate granule neurons is interrupted at an early postmitotic stage supporting a function of *Bcl11b* during postnatal neuronal differentiation. To explore whether loss of *Bcl11b* expression causes indirect phenotypes of the dentate gyrus, we analysed the expression of markers for glial (GFAP), Cajal-Retzius (Reelin) as well as endothelial cells (Pecam). None of the markers exhibits an obvious phenotype in Bcl11b mutants (Supplementary Figure S6A–J).

To address the question whether *Bcl11b* regulates neuronal differentiation cell autonomously or through indirect mechanisms, we generated a mosaic deletion of *Bcl11b* by *ex utero* electroporation of *Cre* recombinase into Bcl11b^flox/flox^ brains at E15.5 followed by organotypic slice culture up to 14 DIV (Figure 4O–S). While there was no significant change in the number of GFP (pCIG2: 6.5 ± 1.12 s.d.; pCIG2-Cre: 6.8 ± 2.3 s.d.) and GFP/*NeuroD* (pCIG2: 2.2 ± 0.8 s.d.; pCIG2-Cre: 2.3 ± 0.8 s.d.) positive cells, we found a significant increase of *NeuroD*-positive cells (pCIG2: 67.9 ± 10.5;
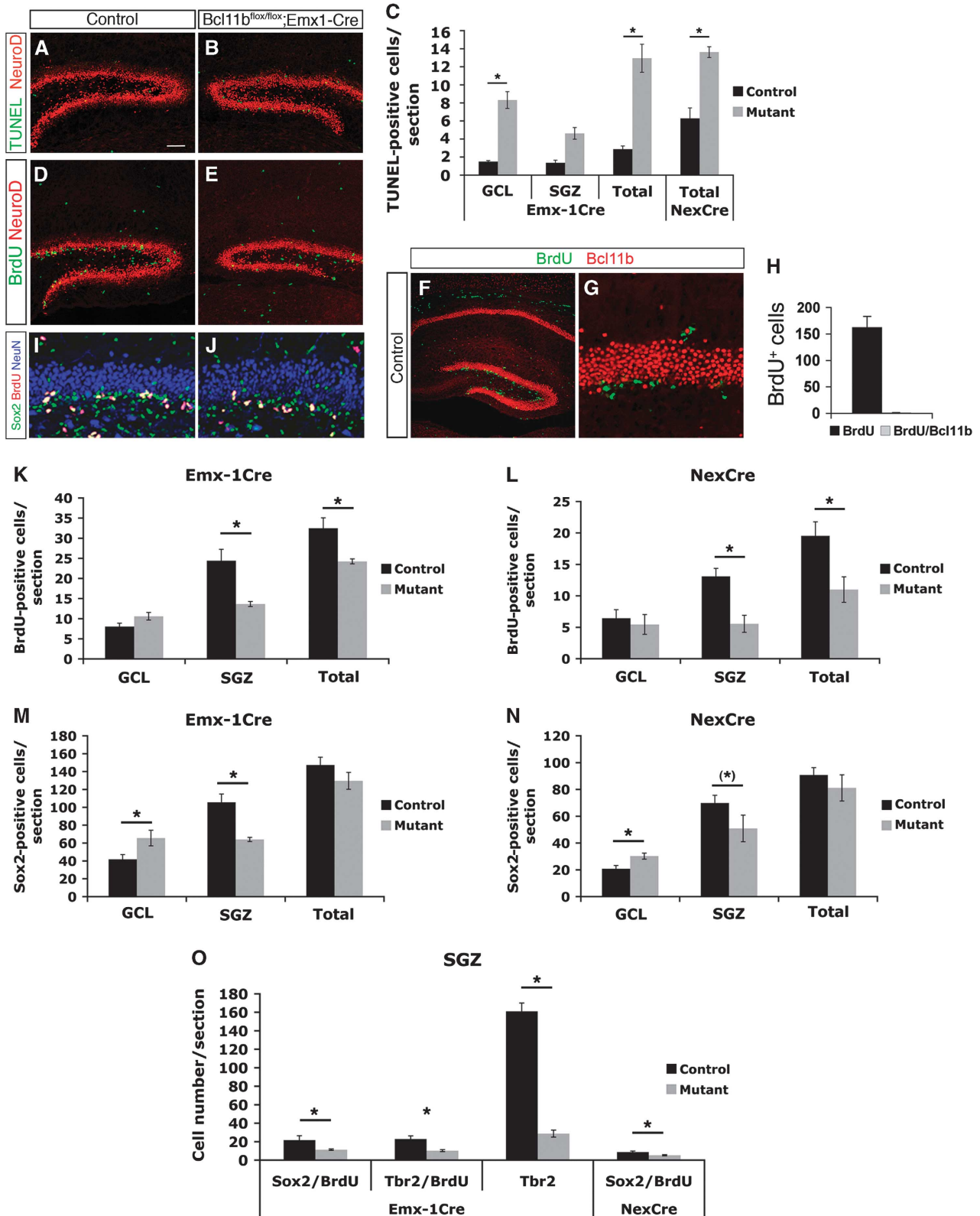
Figure 3 Ablation of *Bcl11b* results in reduced proliferation of progenitor cells, depletion of neural stem cells as well as increased apoptosis. Confocal images of coronal sections of control (**A**, **D**, **F**, **G**, **I**) and *Bcl11b*[flox/flox];Emx1-*Cre* (**B**, **E**, **J**) at P14. Earlier developmental stages are presented in Supplementary Figure S4. Co-staining of TUNEL (green) and *NeuroD* (red) (**A**, **B**); BrdU (green) and *NeuroD* (red) (**D**, **E**); BrdU (green) and *Bcl11b* (red) (**F**, **G**); *Sox2* (green), BrdU (red) and *NeuN* (blue) (**I**, **J**); Statistical analysis of TUNEL assays (**C**), BrdU-positive cells (**K**, **L**) as well as co-staining of *Bcl11b*/BrdU (**H**). (**K–O**) Statistical analysis of *Sox2*- and *Tbr2*-positive cells of control and *Bcl11b* mutant dentate gyrus. *Bcl11b* mutants exhibit a reduced progenitor cell pool and *Sox2* cells are aberrantly located in the granule cell layer in Emx1-*Cre* (**K**, **M**, **O**) as well as NexCre (**L**, **N**, **O**) mutants. *t*-test, *$P<0.05$ error bars, s.e.m. (**C**, **K–O**), s.d. (**H**); $n=3$ (**C**, **H**, **O** (*Tbr2*/BrdU and *Tbr2*)); $n=5$, (**K**, **M**, **O** (*Sox2*/BrdU); $n=6$ (**L**, **N**, **O** (NexCre)). Images taken at ×10 (**A**, **B**, **D–F**), ×40 (**G**, **I**, **J**) magnification. Scale bar: 100 μm (**A**); 20 μm (**H**).
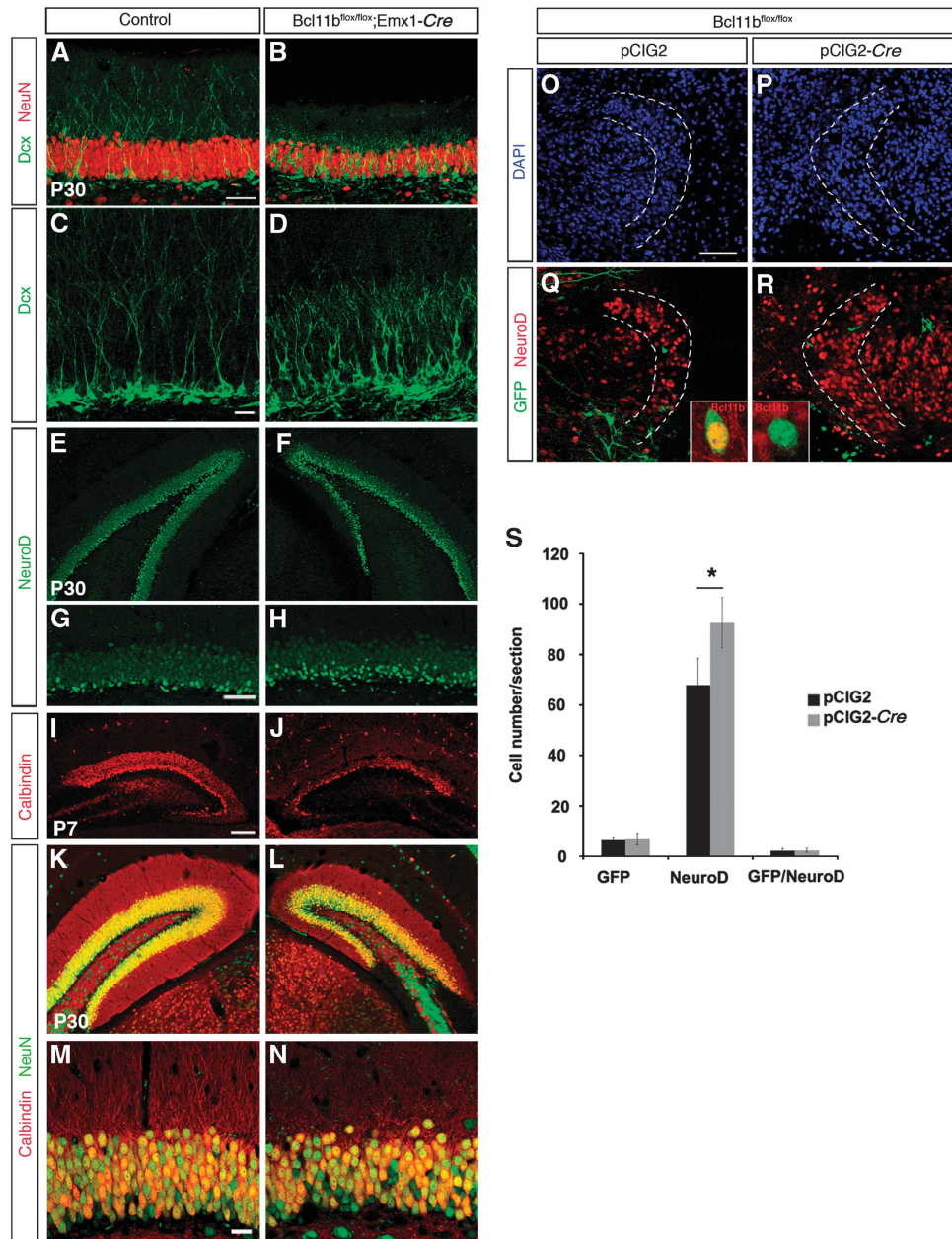
Figure 4 Loss of *Bcl11b* expression disrupts dentate granule cell differentiation. (**A–H**) Immunohistological analysis at P14 of *Dcx* (green) and *NeuN* (red) (**A–D**) as well as *NeuroD* (green) (**E–H**) expression in the dentate gyrus of control (**A, C, E, G**) and *Bcl11b*[flox/flox];Emx1-*Cre* (**B, D, F, H**) animals at P30. (**I–N**) Immunohistological analysis of Calbindin (red) and *NeuN* (green) expression of control (**I, K, M**) and *Bcl11b*[flox/flox]; Emx1-*Cre* (**J, L, N**) granular cells at P7 (**I, J**) and P30 (**K–N**). (**O–S**) Analysis of mosaic deletions of *Bcl11b* by *ex-utero* electroporation of pCIG2 (**O, Q**) and pCIG2-*Cre* (**P, R**) into Bcl11b[flox/flox] brains at E15.5. (**O–R**) Immunohistological analysis after 18 DIV of DAPI (**O, P**) as well as GFP (green) amd NeuroD (red) (**Q, R**). Inserts in (**Q**) and (**R**) demonstrating Bcl11b and GFP expression. (**S**) Statistical analysis of GFP, NeuroD and GFP/NeuroD-positive cells. *t*-test, *$P < 0.005$; error bars, s.d.; $n = 5$. Scale bar: $100 \, \mu m$ (**E, I, P**); $50 \, \mu m$ (**A, G**); $20 \, \mu m$ (**C**).

pCIG2-Cre: 92.6 ± 10; $P < 0.005$) in the mosaic deletion slice cultures (Figure 4S). Thus, deletion of *Bcl11b* in a fraction of dentate neurons suffices to impair neuronal differentiation in surrounding wild-type cells (as determined by the piling-up of *NeuroD* expressing, immature cells), a phenotype that is compatible with indirect functions of *Bcl11b* in neuronal differentiation. This does, however, not exclude additional, direct functions of *Bcl11b* in this process.

We next asked whether the integration of granule cells into the hippocampal circuitry was affected in *Bcl11b* mutants. We used Timm staining to selectively label mossy fibre terminals emanating from the dentate gyrus. Compared with control

hippocampi, we observed highly disorganized projection patterns of mossy fibres in *Bcl11b* mutants (Figure 5A and B), with large amounts of axons travelling aberrantly along the infrapyramidal tract and scattered over the entire pyramidal cell band of the CA3 region. In wild-type animals, mossy fibre axons terminate on characteristic spines, so-called thorny excrescences, on proximal apical dendrites of CA3 neurons (Gonzales *et al*, 2001). In accordance with the aberrant mossy fibre projections, we observed an almost 50% reduction ($P < 0.05$) of thorny excrescences on the proximal apical dendrites of *Bcl11b* mutant CA3 pyramidal cells (Figure 5C).
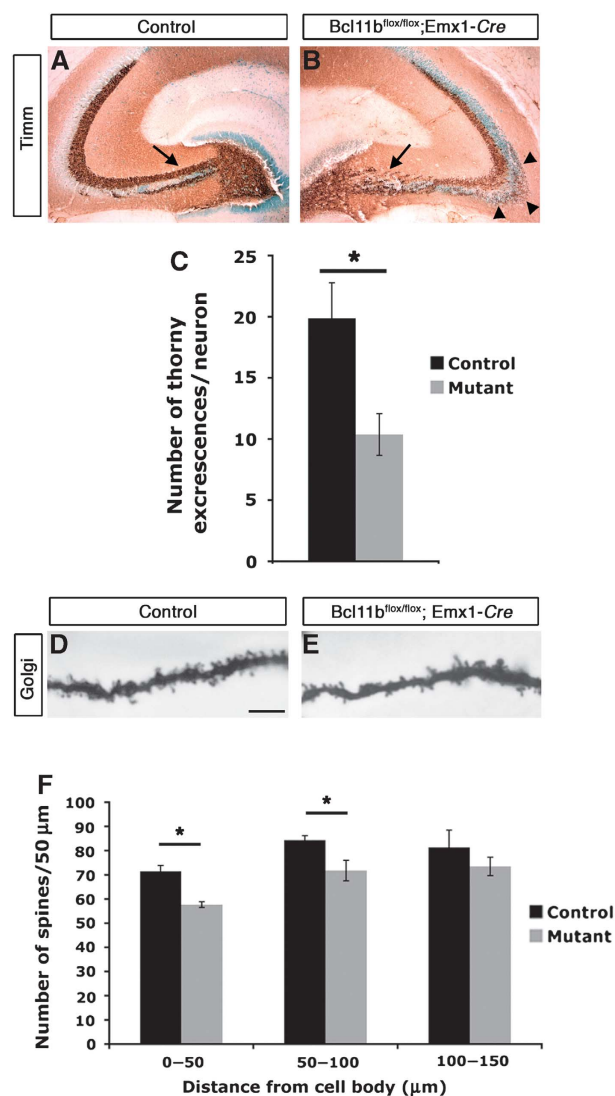
Figure 5 Analysis of granule cell layer processes of *Bcl11b*[flox/flox];
Emx1-*Cre* mice. (**A**, **B**) Timm-stained mossy fibres of adult hippocampi of control (**A**) and *Bcl11b* mutant (**B**) animals. In control animals, the largest part of the mossy fibres of the hilus form synapses on apical dendrites of CA3 neurons (suprapyramidal, arrow) and only a small part runs infrapyramidally. In contrast, *Bcl11b* mutant mossy fibres run mostly infrapyramidally (arrowhead) exhibiting a scattered distribution. (**C**) Statistical analysis of thorny excrescences on apical dendrites of CA3 pyramidal neurons of Golgi impregnated control and *Bcl11b* mutant hippocampi (*t*-test, *$P<0.05$; error bar, s.d.; $n=3$). (**D**, **E**) Golgi stained dendritic spines of control (**D**) and *Bcl11b* mutant (**E**) dentate granule cells. Note dendrites of mutants are shaped and distributed more irregularly. (**F**) Statistical analysis of dendritic spine numbers of control and Bcl11b mutants. Dendrites were subdivided into 50 µm sections starting at the cell soma (*t*-test, *$P<0.05$; error bar, s.d.; $n=3$). Scale bar: 10 µm.

Dentate granule cells receive their major input from the entorhinal cortex. While entorhinal projections strictly terminate along the outer two-thirds of the dendritic tree of a granule cell, commissural as well as associational fibres preferentially project to the inner third close to the cell body (Amaral and Lavenex, 2007). As an indirect measure for the synaptic input to the dentate gyrus, we determined the spine numbers along granule cell dendrites. In *Bcl11b* mutants, dendritic spines as visualized by Golgi impregnation were

shaped and distributed more irregularly as compared with controls (Figure 5D and E). In addition, numbers of spines along the first (next to the soma) and second thirds (middle) of the entire dendrite length were significantly reduced by ~20% ($P<0.05$) and 15% ($P<0.05$), respectively (Figure 5F).

Desmoplakin functions as a direct transcriptional target of Bcl11b

To elucidate a mechanism of *Bcl11b* regulation of neuronal differentiation and progenitor proliferation, we determined target genes by comparative transcriptome analysis using RNA of dentate gyrus tissue harvested from control and mutant animals at P14. We obtained 34 downregulated and 8 upregulated candidate target genes in the *Bcl11b* mutant (Supplementary Table 1) revealing Desmoplakin (*Dsp*) and *Calb1* (downregulated) as well as *HTR2C* and *TacR3* (upregulated) as the most robust target genes. We verified the microarray data for *Dsp* and *Calb1* by RNA *in-situ* hybridization and immunohistochemistry, respectively (Figures 4I–N and 6A–D). Furthermore, immunohistological analysis revealed strong overlap of *Dsp* and *Bcl11b* expression in the dentate gyrus of wild-type animals at P14 but only faint expression of *Dsp* in part of *Sox2*-positive cells (Figure 6E–H). Quantitative RT–PCR determined that expression of *Dsp* and *Calb1* decreases in the mutant by a factor of 14.7 ($P<0.005$) and 4.8 ($P<0.05$), respectively (Figure 6I). *Dsp* was most strongly downregulated in the mutant. Furthermore, we could demonstrate a direct involvement of *Bcl11b* in the regulation of *Dsp* expression by performing chromatin immunoprecipitation (ChIP) on hippocampus tissue of wild-type P14 animals using a *Bcl11b*-specific antibody (Feng and Cooper, 2009; Ganguli-Indra *et al*, 2009) followed by qPCR (Figure 6J). Genomic analysis of the *Dsp* locus by Ensembl.org revealed three potential *Dsp* promoter regions (region1: −315 to +238; region2: +356 to +1194 and region3: +1238 to +1819 corresponding to the transcription start site). Employing several primer pairs for these candidate promoter regions we found that *Bcl11b* is binding to region +479 to +724 relative to the transcription start site of *Dsp* (Figure 6J). The amplified promoter region contains putative *Bcl11b* binding sites GGCCG/AG/AGG (+539 corresponding to the transcription start site; Avram *et al*, 2002) and TGGGC (+539 corresponding to the transcription start site; Cismasiu *et al*, 2006) further supporting the direct activation of *Dsp* expression by *Bcl11b*. Furthermore, employing primer sets covering either both or only the GGCCG/AG/AGG sequence of the potential binding motifs revealed a stronger binding of *Bcl11b* to the *Dsp* promoter region when both motifs were present.

Analysis of the dentate gyrus phenotype of Desmoplakin mutant mice

To further explore the interactions between *Bcl11b* and *Dsp*, we generated forebrain-specific *Dsp* mutants using a floxed *Dsp* allele (Vasioukhin *et al*, 2001). We asked whether *Bcl11b* and *Dsp* mutants exhibit overlapping phenotypes. Morphological analysis of the dentate gyrus of *Dsp*[flox/flox]; Emx1-*Cre* mutants revealed a similar but milder phenotype when compared with *Bcl11b* mutants resulting in reduced size (Figure 7A–C; reduced by 19.6%, $P<0.005$) and cell number (Figure 7F; reduced by 24.5%, $P<0.05$) of the

dentate gyrus as well as granule cell dispersion but to a lesser degree as in *Bcl11b* mutants (Figure 7D and E). Like for *Bcl11b* mutants we found a decrease in the proliferation rate of *Dsp* mutants (Figure 7G–I; reduced by 21.5%, $P<0.05$). *Dsp* mutants unlike *Bcl11b* mutants exhibit a decrease in apoptosis (Figure 7J–L; reduced by 69.1% at P14; $P<0.05$; at P30: control: 5.74 ± 0.74 s.d.; mutant: 3.78 ± 0.39 s.d.; $P<0.05$) suggesting that increased apoptosis as observed in *Bcl11b* mutants is a *Bcl11b*-specific event independent of *Dsp* function. The reduced apoptosis rate of *Dsp* mutants could be responsible for the milder phenotype, especially with regard

to cell dispersion. In addition, *NeuroD* exhibits a similar expression pattern in the *Dsp* mutant when compared with the *Bcl11b* mutant including a 1.4-fold increase of *NeuroD*-positive cells implying a defect in neuronal differentiation (Figure 7M–Q; $P<0.01$). To address whether *Dsp* could rescue the *Bcl11b* phenotype we re-introduced *Dsp* cDNA into *Bcl11b* mutants by *ex-utero* electroporation followed by analysis of the proliferation phenotype (Figure 8A–F). The number of BrdU-positive cells in the *Bcl11b* mutant dentate gyrus electroporated with the empty vector pRC-CMV was reduced by ∼50% compared with *Bcl11b* expressing controls electroporated either with or without empty pRC-CMV (control without electroporation: 22.2 ± 3.7 s.d.; control+ pRC-CMV: 21.6 ± 5.7 s.d.; mutant+pRC-CMV: 12.1 ± 4.7 s.d.; $P<0.01$; Figure 8G). Electroporation of the *Bcl11b* mutant with the *Dsp* expression vector pRC-CMV-*Dsp* resulted in the complete recovery of BrdU-positive cells when compared with the controls (24 ± 5.7 s.d.; Figure 8G). Furthermore, most of the BrdU-positive cells do not colocalize with GFP, providing additional evidence for an indirect regulation of progenitor proliferation by *Bcl11b/Dsp* (Figure 8H).

We next analysed mossy fibre projections in *Dsp* mutants. Compared with controls and *Bcl11b* mutants, *Dsp* mutant animals displayed no overt changes in mossy fibre distribution (Supplementary Figure S7A and B). Taken together, major functions of *Bcl11b* in postnatal hippocampal development, that is, regulation of progenitor cell proliferation as well as neuronal cell differentiation are recapitulated in *Dsp* mutants suggesting *Dsp* to be a functional target of *Bcl11b*. Comparison of mutant phenotypes, however, further indicates that *Bcl11b* acts through additional downstream targets.

Bcl11b involvement in learning and memory
Experimental evidence from our study indicates that ablation of *Bcl11b* expression interferes with the formation of hippocampal circuitry and thus may have an effect on hippocampus-related cognitive and emotional learning and memory. *Bcl11b* control and mutant mice were exposed to the open field test to analyse locomotor (horizontal) activity as well as leaning and rearing (vertical) activity. *Bcl11b* mutants exhibited a significantly higher locomotor and leaning activity whereas rearing activity was significantly lower, a first evidence for a deficit in processing spatial information (Figure 9A–C). Therefore, we tested the spatial learning by
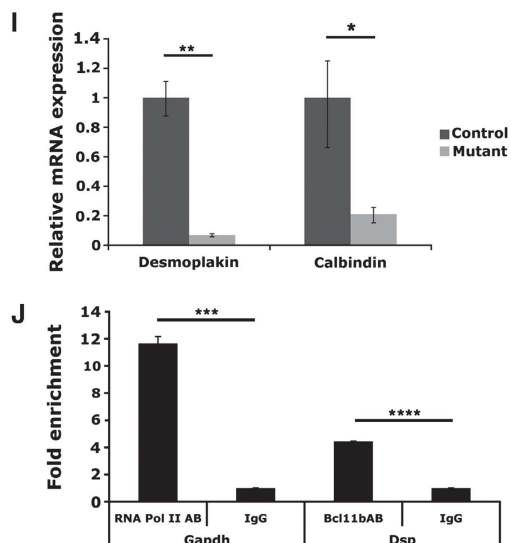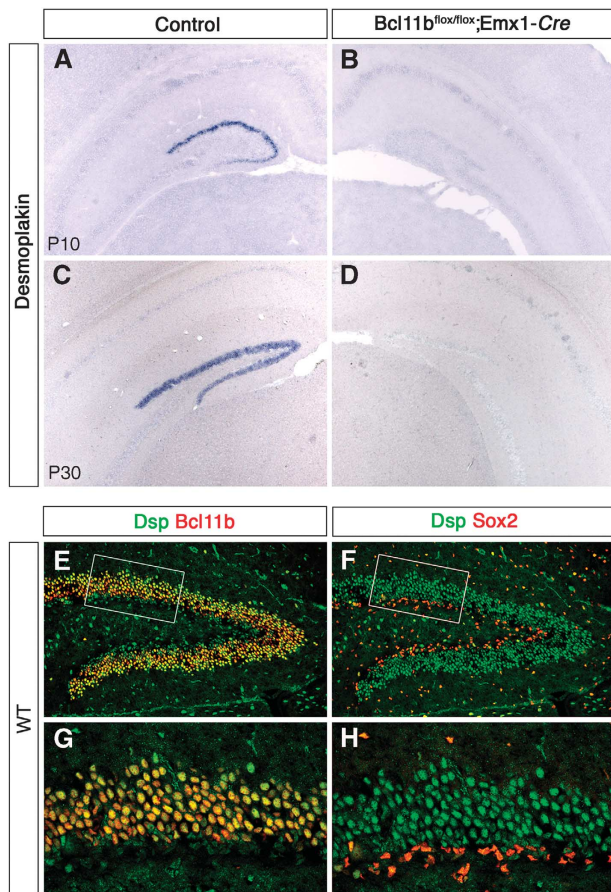

Figure 6 Desmoplakin is a direct transcriptional target of *Bcl11b*. (**A–D**) Desmoplakin RNA *in-situ* hybridization of hippocampal cryostat sections of control (**A, C**) and *Bcl11b*^flox/flox;Emx1-*Cre* (**B, D**) animals at P10 (**A, B**) and P30 (**C, D**). (**E–H**) Co-expression analysis of *Dsp* (green) and *Bcl11b* (red) (**E, G**) as well as *Sox2* (red) (**F, H**) of wild-type dentate gyrus at P14. Images taken at ×20 (**E, F**) and ×63 (**G, H**) magnification. Scale bars: 100 µm (**E**); 20 µm (**G**). (**I**) Determination of hippocampal relative mRNA expression levels of Desmoplakin and Calbindin by quantitative RT–PCR at P14 ($2^{-\Delta\Delta C_T}$ method; *t*-test, *$P<0.05$; **$P<0.005$; error bar, s.d.; $n=4$). (**J**) Determination of direct interaction of *Bcl11b* and Desmoplakin by Chromatin immunoprecipitation (ChIP). ChIP assays were performed on hippocampus tissue of P14 animals employing a *Bcl11b*-specific antibody (Bcl11bAB), IgG as a negative control and an RNA polymerase II (RNA Pol II AB)-specific antibody as positive control. Direct interactions were determined by qPCR using specific primer pairs for Desmoplakin regulatory regions as well as a specific primer pair for the *Gapdh* promoter region ($2^{-\Delta\Delta C_T}$ method; *t*-test, ***$P<0.001$; ****$P<0.0001$; error bar, s.d.; hippocampi of 10 animals were used per assay).
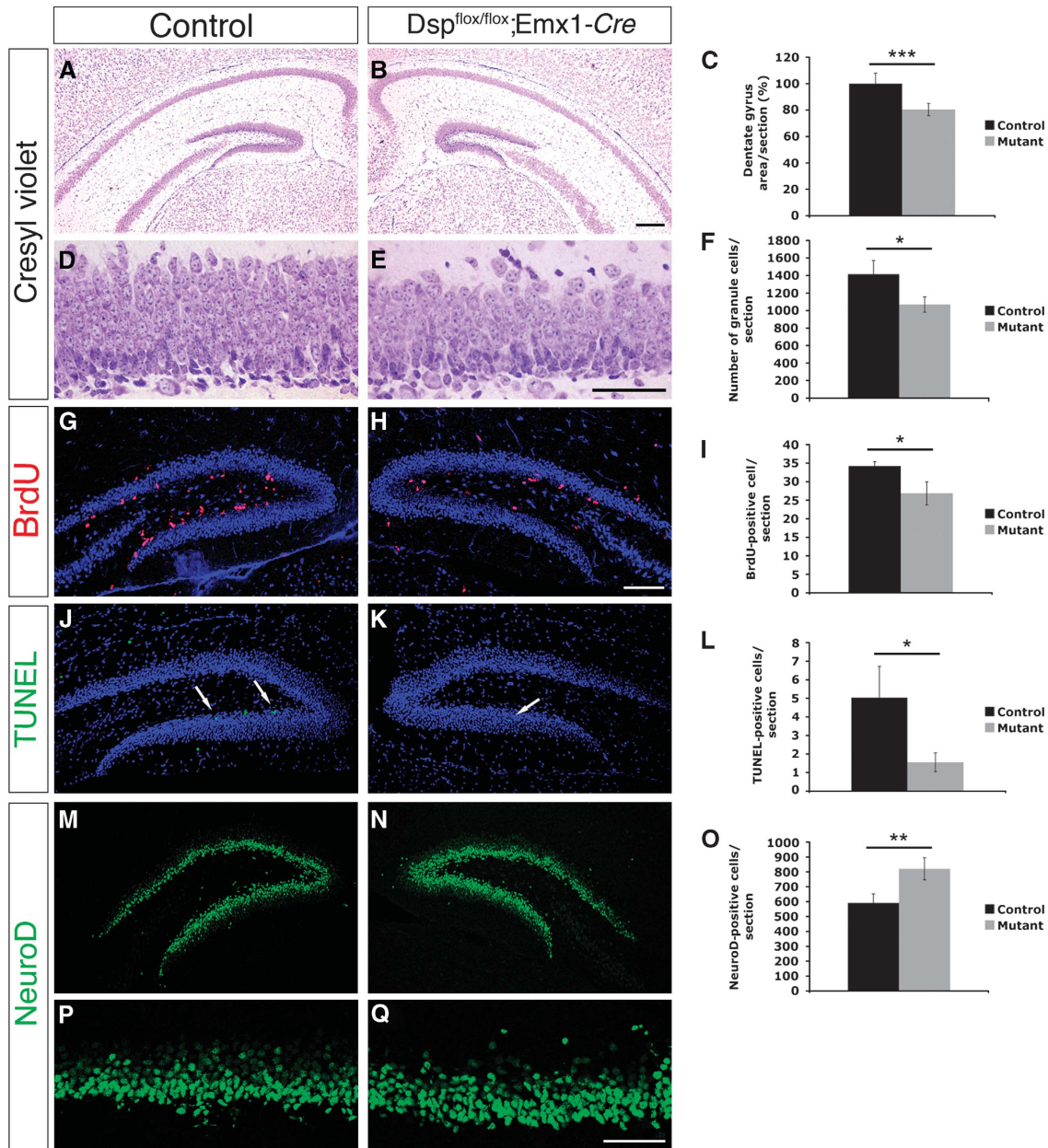
Figure 7 Analysis of the hippocampus-specific *Dsp*^flox/flox;Emx1-*Cre* phenotype at P14. (**A–F**) Morphological analysis by cresyl-violet staining of control (**A**, **D**) and *Dsp*^flox/flox;Emx1-*Cre* (**B**, **E**) coronal forebrain sections as well as statistical analysis of the dentate gyrus area (**C**) and cell number (**F**). (**G–I**) Immunohistochemical analysis of progenitor proliferation by BrdU incorporation of control (**G**) and *Dsp*^flox/flox;Emx1-*Cre* (**H**) animals. BrdU, red; *NeuN*, blue. (**J–L**) Analysis of cell death of control (**J**) and *Dsp*^flox/flox;Emx1-*Cre* (**K**) by TUNEL assay. TUNEL, green; DAPI, blue; arrows indicate TUNEL-positive cells. (**M–Q**) Immunohistochemical analysis of *NeuroD* (green)-positive cells in control (**M**, **P**) and *Dsp*^flox/flox;Emx1-*Cre* (**N**, **Q**) animals (*t*-test, *$P<0.05$; **$P<0.01$; ***$P<0.005$; error bar, s.d.; $n=4$ (**C**, **F**); $n=3$ (**I**, **L**, **O**)). Scale bar: 250 µm (**B**), 100 µm (**H**), 50 µm (**E**, **Q**).

exposing control and *Bcl11b* mutant animals to a spatial eight-arm radial maze test. Spatial working memory capacity was determined by counting the number of errors, for example, re-entering an already entered arm. Both control and mutant animals demonstrated a significant decrease in the number of errors until day 3 of the experiment (Figure 9D; *$P<0.05$; **$P<0.005$; ***$P<0.0005$; ****$P<0.0001$). During the whole testing period, *Bcl11b* mutants exhibited significantly higher numbers of working memory errors compared with control animals. The results demonstrate a reduced learning capability of the *Bcl11b* mutants compared

with control animals with the number of errors ~7 times higher for the mutant on the last 3 days of training (ANOVA: *F*-value $(1,16)=28.575$ (sample), $P<0.001$; *F*-value $(4,16)=7.297$ (day), $P<0.001$).

This is supported by the fact that in mutants the number of new arm entries during the first eight-arm entries was not different from a random sequence, indicating low, if any learning. In contrast, wild-type mice continuously enhanced the number of new entries during the trials indicating good spatial learning performance (Figure 9E; mutants: 5.1 ± 0.24; wild type: 6.9 ± 0.22; $P=0.00001$).
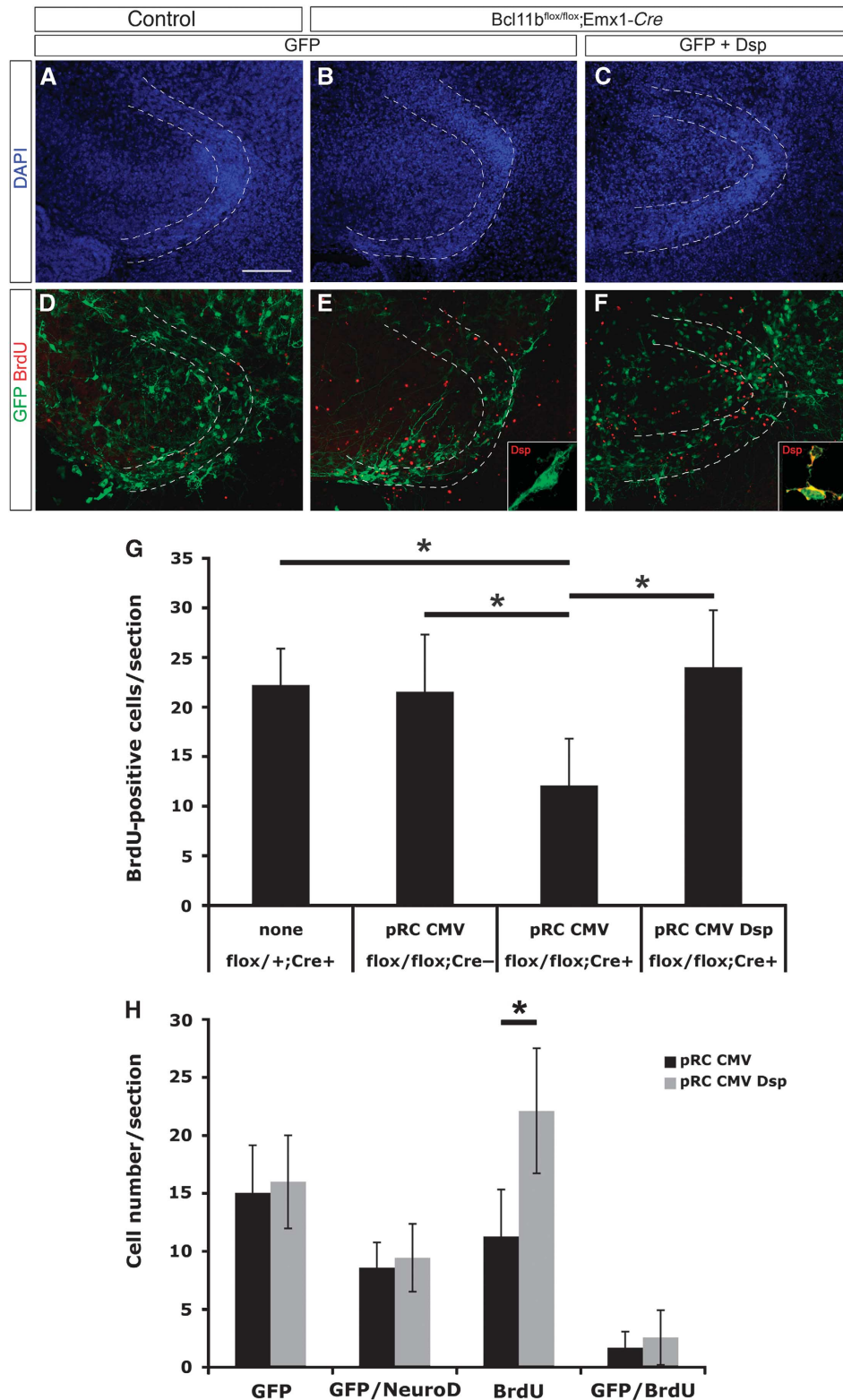
Figure 8 Re-introduction of Desmoplakin expression rescues *Bcl11b* phenotype. (**A–F**) Immunohistological analysis of control (**A**, **D**) and Bcl11b^flox/flox;Emx1-*Cre* (**B**, **C**, **E**, **F**) hippocampal slice cultures after 11 DIV electroporated with control pRC-CMV (**A**, **B**, **D**, **E**) and pRC-CMV-*Dsp* (**C**, **F**) expression vectors as well as vector pCAGGS expressing GFP using DAPI (blue) as morphological marker, GFP (green) as marker for electroporation efficiency and BrdU (red) as marker for cell proliferation. Inserts in (**E**) and (**F**) showing *Dsp* and GFP expression. Images taken at ×20 magnification. (**G**) Statistical analysis of BrdU-positive cells in control and mutant hippocampal slice cultures. (**H**) Statistical analysis of co-expression of GFP/*NeuroD*- and GFP/BrdU-positive cells (*t*-test, *$P < 0.01$; error bar, s.e.m.; $n = 4$).
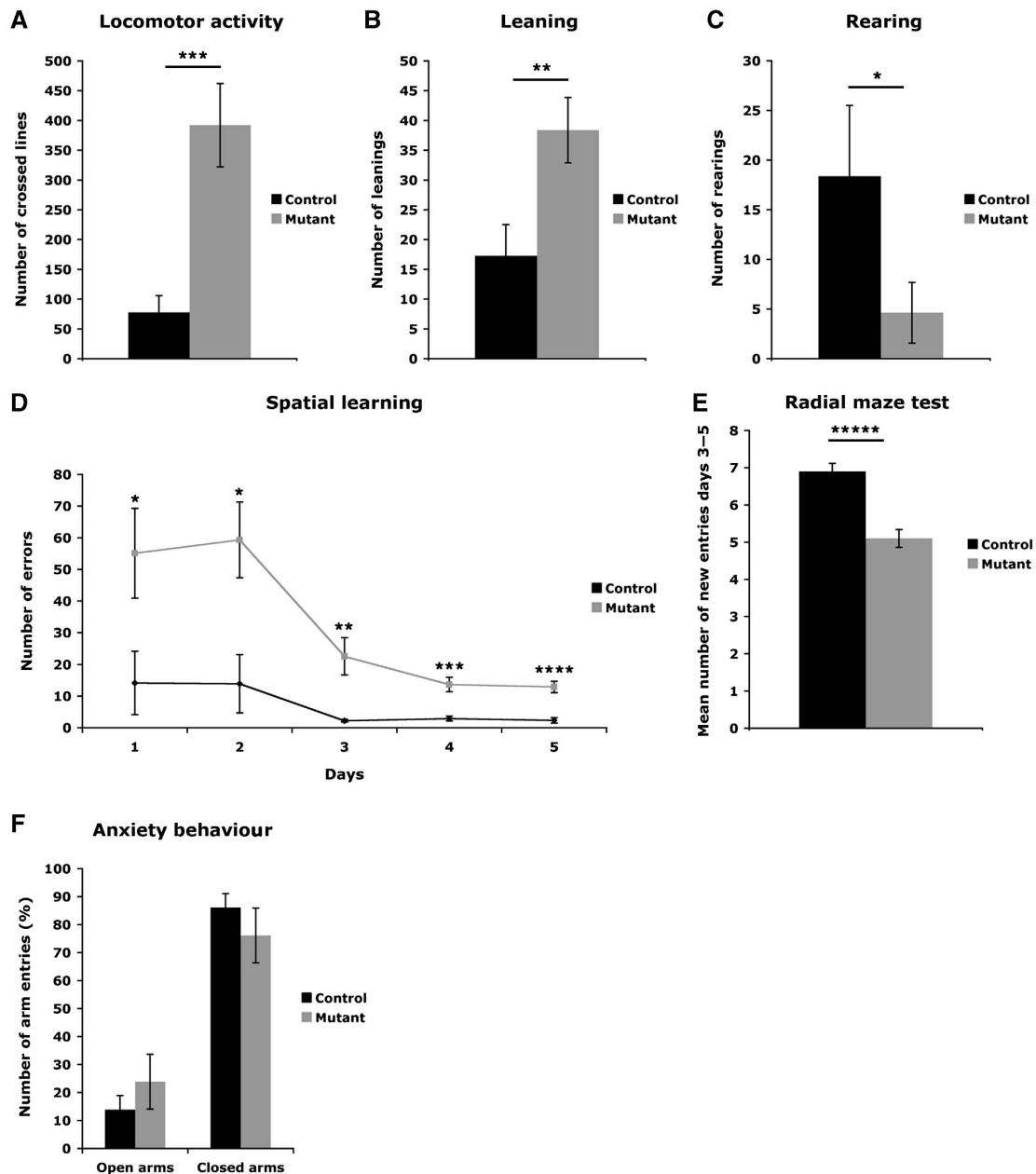
Figure 9 Ablation of *Bcl11b* causes impaired learning and memory behaviour. (**A–C**) Open field test analysing locomotor activity (**A**), leaning (**B**) and rearing (**C**) behaviour (*t*-test, *$P = 0.01$; **$P = 0.0005$; ***$P = 0.00001$; error bar, s.e.m.; $n = 8$). (**D, E**) Radial maze test analysing spatial learning behaviour by determining the number of errors at 5 successive days (*t*-test, *$P < 0.05$; **$P < 0.005$; ***$P = 0.0005$; ****$P = 0.0001$; error bar, s.e.m.; $n = 9$) (**D**) and number of entries into new radial arms of days 3–5 (*t*-test, *****$P < 0.00001$; error bar, s.e.m.; $n = 9$) (**E**). (**F**) Elevated plus maze test analysing anxiety behaviour by determining number of arm entries in relation to locomotor activity. No significant differences between control and mutant animals were observed ($n = 9$).

Bcl11b is also expressed in the amygdala (Leid *et al*, 2004) a brain region related to fear- and anxiety-memory processing. To exclude that the learning and memory deficits observed in the *Bcl11b* mutants are related to lack of *Bcl11b* expression in the amygdala, we tested the anxiety-related behaviour of *Bcl11b* mutants in an elevated plus maze experiment. Animals exhibiting increased anxiety avoid the entry into unprotected arms. *Bcl11b* mutant animals again exhibited a high locomotor activity but no significant difference in entering protected or unprotected arms between control and mutant animals, suggesting that there is no difference in

anxiety-related behaviour (Figure 9F). Although *Dsp* is a functional target of *Bcl11b* with respect to cell proliferation and differentiation *Dsp* mutants did not exhibit behavioural impairments in open field and radial maze tests (Supplementary Figure S7C–G). Although there is no significant difference in the spatial learning behaviour of control and mutant animals *Dsp* mutant animals have the tendency to be more explorative but unable to consolidate the information (Supplementary Figure S7F and G). These data in accordance with the unchanged mossy fibres of *Dsp* mutants suggest a *Dsp*-independent role of *Bcl11b* in learning and memory.

Discussion

In this study, we demonstrate that *Bcl11b/Ctip2* is required for structural as well as functional development of the dentate gyrus. Functions of *Bcl11b* are phase specific and restricted to the postnatal period of dentate development: (i) *Bcl11b* controls progenitor cell proliferation and the size of the neural stem-cell compartment in the dentate gyrus through indirect mechanisms. In addition, loss of *Bcl11b* expression increases apoptosis of postmitotic neurons. Thus, mutation of *Bcl11b* leads to a hypoplastic dentate gyrus with reduced numbers of granule cells. (ii) *Bcl11b* is further required for cell type-specific differentiation of dentate granule neurons. In the absence of *Bcl11b*, newborn neurons are arrested at early differentiation levels, colonizing the residual GCL. (iii) *Bcl11b* is essential for functional integration of granule cells into hippocampal circuitry. In *Bcl11b* mutant granule cells, both synaptic input as reflected by reduced dendritic spine numbers, and synaptic output as reflected by aberrant mossy fibre projections and reduced thorny excrescences on CA3 neurons (Gonzales *et al*, 2001), are impaired. This results in reduced spatial learning capacities in Bcl11b mutants.

Finally, we found Desmoplakin to be a direct transcriptional target of *Bcl11b* in dentate granule cells, and demonstrate that *Bcl11b* binds directly to regulatory sequences in close proximity to the transcription start site of *Dsp*, which includes putative *Bcl11b* binding sites (Avram *et al*, 2002; Cismasiu *et al*, 2006). Furthermore, re-introducing *Dsp* expression into the *Bcl11b* mutant dentate gyrus rescues the progenitor proliferation phenotype. This is in accordance with previous reports defining a role of *Dsp* in stem-cell proliferation (Gallicano *et al*, 1998). Comparing *Bcl11b* and *Dsp* mutant hippocampi, we were able to separate functions of *Bcl11b* depending on *Dsp* expression from those independent of *Dsp* and likely involving additional, yet undetermined signals.

Bcl11b in hippocampal neurogenesis

We found that *Bcl11b* expression in the dentate gyrus is restricted to postmitotic neurons. In addition, at embryonic stages we could not detect *Bcl11b* expression in migrating progenitor cells contributing to the dentate primordium. Thus, impaired progenitor cell proliferation and depletion of the neural stem-cell pool, as defined by BrdU incorporation, and reduction of *Sox2/Tbr2* expressing cells (Kempermann *et al*, 2004; Englund *et al*, 2005; Li *et al*, 2009) are most likely caused by a lack of indirect feedback signals from postmitotic neurons, no longer expressing *Bcl11b*. Analysing *Bcl11b*flox/flox;*NexCre* mice, where *Cre*-recombinase is only active in postmitotic cells (Goebbels *et al*, 2006; Seuntjens *et al*, 2009), further supports this hypothesis. Although we cannot exclude that the observed increase in apoptosis could contribute in part to the depletion of the neural stem-cell pool we found most apoptotic cells were located in the GCL. These data suggest that *Sox2*-positive cells aberrantly migrating to the GCL may loose their proliferation capacity and are unable to complete the differentiation process. Instead these cells undergo apoptosis. Indirect control of hippocampal stem cells was recently demonstrated for the transcription factor *Sox2* as well. Unlike *Bcl11b*, *Sox2* is expressed by neural stem cells regulating the maintenance of the dentate stem-cell niche through *Wnt3a* and *Shh* signals

(Favaro *et al*, 2009). Previous reports suggest that *Bcl11b* interacts directly with members of the cyclin-dependant kinase inhibitor family, for example, *p21WAF1* and *p57KIP2* (Topark-Ngarm *et al*, 2006; Cherrier *et al*, 2009). p57KIP2 is an important regulator of the cell cycle and neuronal differentiation. During early embryogenesis, *p57KIP2* is expressed in newly differentiated neurons but not in the proliferative ventricular zone (Yan *et al*, 1997). *Bcl11b* directly represses *p57KIP2* expression in Sk-N-MC neuronal cells resulting in impaired neuronal differentiation (Topark-Ngarm *et al*, 2006). Control of neurogenesis in the dentate gyrus through *Bcl11b*-dependent regulation of *p57KIP2* levels would require active repression of *p57KIP2* by *Bcl11b* in proliferating progenitors, which is not supported by our expression analysis of *Bcl11b*.

Dsp mutant mice exhibit a similar although weaker phenotype when compared with *Bcl11b* mutants, for example, smaller dentate gyrus, and reduced proliferation rate suggesting that *Dsp* acts downstream of *Bcl11b* in these processes. Complete recovery of the proliferation phenotype by re-introducing *Dsp* expression into *Bcl11b* mutants further demonstrates an important role of *Dsp* in progenitor cell proliferation. This coincides with a previous report demonstrating that ablation of *Dsp* expression causes reduced proliferation during early embryonic development (Gallicano *et al*, 1998). The weaker Dsp phenotype might be due to the decrease in apoptosis in the *Dsp* mutant in contrast to the increase in apoptotic cells in *Bcl11b* mutants. However, this does not exclude additional factors to be involved.

There is emerging evidence that cell–cell adhesion is important for the control of stem-cell behaviour and the transmission of regulatory signals provided to the stem-cell niche (Marthiens *et al*, 2010; Redmer *et al*, 2011), raising the possibility that *Dsp* may exert similar functions in the control of hippocampal neurogenesis. As mentioned above, *Dsp* expression rescues the *Bcl11b* proliferation phenotype. In addition, we observed a misdistribution of *Sox2*-positive cells, for example, loss of *Sox2*-positive cells in the SGZ and increase of *Sox2*-positive cells in the GCL, suggesting that stem cells leave the stem-cell niche but are not able to further differentiate. It is possible that *Dsp* is required to provide cell–cell adhesion in order to establish the signalling pathway from neighbouring cells to allow neuronal differentiation (see also below).

Bcl11b in neuronal differentiation

We found that *Bcl11b* is required for cell type-specific differentiation of dentate granule cells. Previous reports demonstrated similar regulatory functions for *Bcl11b* in the development of corticospinal motor neurons and the striatum (Arlotta *et al*, 2005, 2008). Outside the CNS, *Bcl11b* is critical for the differentiation of T lymphocytes (Wakabayashi *et al*, 2003; Liu *et al*, 2010), suggesting the regulation of cellular differentiation to be a conserved function of *Bcl11b*. Surprisingly, our mosaic deletion data suggest a non-cell autonomous role of *Bcl11b* in the regulation of neuronal differentiation, and deletion of *Bcl11b* in a fraction of dentate neurons leads to impaired neuronal differentiation in surrounding wild-type cells. It was shown that *Bcl11b* plays an important non-cell autonomous role in the proliferation and differentiation of keratinocytes, suggesting that *Bcl11b*

regulates transcription of secreted dermal factors including KGF, a dermal fibroblast-derived growth factor, which in turn regulates epidermal morphogenesis in a paracrine fashion (Golonzhka et al, 2009). This is also supported by a recent report demonstrating a non-cell autonomous role for Bcl11b in tissue formation during wound healing that is most likely due to impaired cell–cell adhesion and might include the regulation of E- and P-cadherin (Liang et al, 2012). From our data, we conclude that Bcl11b regulates progenitor proliferation as well as differentiation in a non-cell autonomous fashion but that different additional factors might be involved in the regulation of these processes. We cannot exclude that Bcl11b, in addition, has a cell autonomous function in neuronal differentiation. Defective differentiation of dentate granule cells was also observed in Dsp mutants. Dsp interacts with desmosomal cadherins via plakoglobin connecting desmosomes with intermediate filaments of the cytoskeleton (Garrod and Chidgey, 2008). The cytoskeleton plays an important role in cell division, cell polarity and cell differentiation as well as signalling (Hoogenraad and Bradke, 2009). In the epidermis, Dsp rearranges microtubules according to the differentiation state of the cell (Lechler and Fuchs, 2007). Thus, it is possible that Dsp has a similar function in neuronal cells. Lack of Bcl11b and Dsp expression could therefore cause defects in the organization of the cytoskeleton resulting in granule cell dispersion as well as in impaired neuronal differentiation. Further, indirect evidence for an interaction between Bcl11b and Dsp was provided by Bcl11b regulation of proliferation and late differentiation in keratinocytes where Dsp expression occurs (Golonzhka et al, 2007, 2009).

Ablation of Bcl1b in the hippocampus caused aberrant mossy fibre projections and severe deficits in spatial learning and memory. None of these mutant phenotypes was recapitulated in Dsp mutants. This indicates that major functions of Bcl11b in hippocampal development occur independent of Dsp. Furthermore, it suggests that the failure of Bcl11b mutant granule neurons to integrate into the hippocampal circuitry is critical for the development of learning and memory deficits (Schwegler et al, 1990; Schwegler and Crusio, 1995).

Perspectives
Regulation of the developing dentate gyrus is of special interest because it is one of only two brain regions with ongoing neurogenesis in adulthood. Expression of Bcl11b in the dentate gyrus is sustained throughout the life (LB, RS and SB, unpublished). It will be interesting to determine whether Bcl11b executes a similar function during neurogenesis of the adult and aged hippocampus. Dysregulated neurogenesis is associated with disorders like Alzheimer's disease and Schizophrenia (Zhao et al, 2008; Clelland et al, 2009; DeCarolis and Eisch, 2010). Bcl11b with its dual phase-specific regulatory functions during postnatal development can provide an excellent model system to gain better insight into the mechanisms of learning and memory and the pathophysiology of associated diseases.

Materials and methods

Animals
For the generation of a conditional knockout allele, exons 4–6 of the Bcl11b gene and exon 2 of the Dsp gene were floxed as described previously (Vasioukhin et al, 2001; Li et al, 2010). Bcl11b^flox/flox as well as Dsp^flox/flox mice were crossed to Emx1-Cre (Gorski et al, 2002) as well as to NexCre (Goebbels et al, 2006) transgenic mice. To exclude Cre-related effects, homozygous mutant mice were strictly compared with heterozygous controls harbouring a Cre allele. Genotyping of the mice was performed by PCR. All animal experiments were carried out in accordance with the German law and were approved by the respective government offices in Berlin, Göttingen and Tübingen.

In-situ hybridization, histology, immunohistology, Timm staining and Golgi impregnation
For in-situ hybridization, forebrains were dissected from control and mutant embryos at E15 and E18 as well as animals at P7, P10, P14 and P30, fixed with 4% PFA and embedded in OCT compound (Sakura). Hybridizations were performed with DIG-labelled ribo-probes on 18 μm cryosections.

For immunofluorescence staining, brain tissues were fixed with 4% PFA in 0.1 M sodium phosphate buffer (pH 7.4). In all, 14 μm cryosections were obtained from matched control and mutant brains. Stained sections were examined on a confocal microscope (Zeiss LSM510, or Leica Sp5II).

For the Timm staining, mice were transcardially perfused with buffered sodium sulphate and glutaraldehyde, placed overnight in a 30% saccharose solution followed by embedding in OCT compound (Sakura). In all, 40 μm sections were developed in Timm's solution and counterstained with methylene blue as was described in Schwegler and Lipp (1983).

Golgi staining of hippocampal tissue was carried out according to a modified protocol published previously (Heimrich and Frotscher, 1991).

Morphological analysis was performed on 5 μm methacrylat sections (Technovit 7100, Heraeus-Kulzer, Wehrheim, Germany) using 0.02% cresyl violet/0.2 M Walpole buffer (Chroma-Waldeck, Münster, Germany) for 30 min at room temperature.

Antibodies
The following antibodies were used: Goat anti-NeuroD and anti-Dcx as well as mouse anti-NeuN (all from Santa Cruz), rabbit anti-Calbindin (Swant), rabbit anti-Sox2 as well as mouse anti-Reelin (all from Millipore), rat anti-BrdU (AbD Serotec), mouse anti-GFAP (Sigma-Aldrich), rabbit anti-Pecam and anti-Tbr2 (Abcam) and rabbit anti-Dsp (E Fuchs, Rockefeller University). To generate an anti-Bcl11b serum, a 519-bp fragment from the murine Bcl11b cDNA, corresponding to aa 462–634 (NM_021399) was amplified by PCR. The PCR fragment was cloned into the bacterial expression vector pET-14b (Novagen), which provided coding sequences for a His6 tag. His6-Bcl11b was propagated in BL21(DE3)pLysS cells, affinity purified on TALON metal resin (BD Biosciences) and injected into rabbits and guinea pigs (Charles River).

Ex-utero electroporation and slice culture
Slice cultures of Bcl11b^flox/flox;Emx-1Cre as well as Bcl11b^flox/flox embryonic brains were carried out as described (Hand et al, 2005). Briefly, 4 μg of DNA was electroporated into the prospective dentate gyrus area of embryonic brains at E 15.5 using five pulses at 50 V, brains were cut into 250 μm slices and kept in culture up to 11 DIV (rescue experiments) or 18 DIV (mosaic experiments). To determine the proliferation rate of dentate gyrus cells, BrdU (10 μM) was added to the culture medium for the first 20 h after electroporation. For the rescue experiments, brains were electroporated with the vectors pRC-CMV, pRC-CMV-Dsp (Koeser et al, 2003), as well as with pCAGGS for GFP expression. For mosaic experiments, pCIG2 and pCIG2-Cre vectors were used (Hand et al, 2005).

Determination of progenitor cell proliferation and apoptosis
Progenitor cell proliferation was determined by BrdU incorporation. Pregnant females or pups at the indicated times were injected with BrdU (100 μg/g body weight; Sigma-Aldrich, cat. #: B9285) 2 h before tissue dissection. Apoptotic cells were detected by TUNEL assay according to manufacturer's manual (Millipore, cat. #: S7110).

Determination of dentate gyrus cell number and area
Forebrain tissues from at least three mutant and control animals were sectioned serially (14 μm thickness). Dentate gyrus cell number and area were determined on three or nine matched sections of the caudal, medial as well as the rostral hippocampus per animal

and the average value of a section per animal was determined. Values were presented as means ± s.e.m (*Bcl11b*) or ± s.d (*Dsp*). Differences in values were considered to be significant at $P < 0.05$ by Student's *t*-test.

Determination of the number of dendritic spines and thorny excrescences

Sections of three Golgi impregnated control and *Bcl11b* mutant hippocampi were used to determine the dendritic spine number of the dorsal and ventral dentate gyrus granule cells as well as the thorny excrescences located in the apical dendritic tree of CA3 pyramidal neurons. At least 15 neurons and a total of 7000 spines per animal were counted. To determine the dendritic spine number, selected dendrites were divided into 50 μm sections starting from the cell soma to the end of the dendrites. The spines of 30 dendrites per animal were counted. Thorny excrescences were identified according to previously published morphological criteria (Gonzales *et al*, 2001) and counted within the first 50 μm from the soma of the apical dendrites of CA3 pyramidal cells corresponding to the stratum lucidum. At least 7–10 neurons per animal and 200 thorny spines per neuron were counted. Values were presented as means ± s.d. differences in values were considered to be significant at $P < 0.05$ by Student's *t*-test.

Microaray analysis, quantitative real-time RT–PCR and ChIP of Bcl11B target genes

Microarray analysis, quantitative RT–PCR as well as ChIP assays are described elsewhere (John *et al*, 2012). For detailed information, see Supplementary Material and methods.

Behavioural tests

Behavioural analysis was performed employing adult male as well as female wild-type and mutant animals to open field ($n = 8$), elevated plus maze ($n = 9$) and radial arm maze ($n = 9$) tests. Control and mutants were age matched and of the same genetic background (Bl6/CD1). Open field, elevated plus maze as well as radial arm maze tests are described elsewhere (Schwegler *et al*, 1990; Yilmazer-Hanke *et al*, 2004). For detailed information, see Supplementary Material and methods.

Statistical analysis

Results are expressed as the mean ± s.e.m. or ± s.d. Comparisons between groups were made by an unpaired two-tailed Student's *t*-test or analysed using the $2^{-\Delta\Delta C_T}$ method as described previously (Livak and Schmittgen, 2001) (quantitative real-time RT–PCR). *Sox2*

and BrdU double-labelled cells were analysed by one-tailed Student's *t*-test. A two-way ANOVA with dependent variables was performed for the analysis of the radial maze data.

Supplementary data

Supplementary data are available at *The EMBO Journal* Online (http://www.embojournal.org).

Conflict of interest

The authors declare that they have no conflict of interest.

References

Altman J, Bayer SA (1990) Migration and distribution of two populations of hippocampal granule cell precursors during the perinatal and postnatal periods. *J Comp Neurol* **301:** 365–381

Amaral DG, Lavenex P (2007) Hippocampal Neuroanatomy. In *The Hippocampus Book*, Andersen P, Morris R, Amaral DG, Bliss T, O'Keefe J (eds), Vol. 3, pp 37–114. New York: Oxford University Press

Arlotta P, Molyneaux BJ, Chen J, Inoue J, Kominami R, Macklis JD (2005) Neuronal subtype-specific genes that control corticospinal motor neuron development *in vivo*. *Neuron* **45:** 207–221

Arlotta P, Molyneaux BJ, Jabaudon D, Yoshida Y, Macklis JD (2008) Ctip2 controls the differentiation of medium spiny neurons and the establishment of the cellular architecture of the striatum. *J Neurosci* **28:** 622–632

Avram D, Fields A, Senawong T, Topark-Ngarm A, Leid M (2002) COUP-TF (chicken ovalbumin upstream promoter transcription factor)-interacting protein 1 (CTIP1) is a sequence-specific DNA binding protein. *Biochem J* **368:** 555–563

Chen B, Wang SS, Hattox AM, Rayburn H, Nelson SB, McConnell SK (2008) The Fezf2-Ctip2 genetic pathway regulates the fate choice of subcortical projection neurons in the developing cerebral cortex. *Proc Natl Acad Sci USA* **105:** 11382–11387

Cherrier T, Suzanne S, Redel L, Calao M, Marban C, Samah B, Mukerjee R, Schwartz C, Gras G, Sawaya BE, Zeichner SL, Aunis D, Van Lint C, Rohr O (2009) p21(WAF1) gene promoter is epigenetically silenced by CTIP2 and SUV39H1. *Oncogene* **28:** 3380–3389

Cismasiu VB, Ghanta S, Duque J, Albu DI, Chen HM, Kasturi R, Avram D (2006) BCL11B participates in the activation of IL2 gene expression in CD4 + T lymphocytes. *Blood* **108:** 2695–2702

Clelland CD, Choi M, Romberg C, Clemenson Jr. GD, Fragniere A, Tyers P, Jessberger S, Saksida LM, Barker RA, Gage FH, Bussey TJ (2009) A functional role for adult hippocampal neurogenesis in spatial pattern separation. *Science* **325:** 210–213

DeCarolis NA, Eisch AJ (2010) Hippocampal neurogenesis as a target for the treatment of mental illness: a critical evaluation. *Neuropharmacology* **58:** 884–893

Desplats PA, Lambert JR, Thomas EA (2008) Functional roles for the striatal-enriched transcription factor, Bcl11b, in the control of striatal gene expression and transcriptional dysregulation in Huntington's disease. *Neurobiol Dis* **31:** 298–308

Englund C, Fink A, Lau C, Pham D, Daza RA, Bulfone A, Kowalczyk T, Hevner RF (2005) Pax6, Tbr2, and Tbr1 are expressed sequentially by radial glia, intermediate progenitor cells, and postmitotic neurons in developing neocortex. *J Neurosci* **25:** 247–251

Favaro R, Valotta M, Ferri AL, Latorre E, Mariani J, Giachino C, Lancini C, Tosetti V, Ottolenghi S, Taylor V, Nicolis SK (2009) Hippocampal development and neural stem cell maintenance require Sox2-dependent regulation of Shh. *Nat Neurosci* **12:** 1248–1256

Feng L, Cooper JA (2009) Dual functions of Dab1 during brain development. *Mol Cell Biol* **29:** 324–332

Ferri AL, Cavallaro M, Braida D, Di Cristofano A, Canta A, Vezzani A, Ottolenghi S, Pandolfi PP, Sala M, DeBiasi S, Nicolis SK (2004) Sox2 deficiency causes neurodegeneration and impaired neurogenesis in the adult mouse brain. *Development* **131:** 3805–3819

Frotscher M, Zhao S, Forster E (2007) Development of cell and fiber layers in the dentate gyrus. *Prog Brain Res* **163:** 133–142

Gallicano GI, Kouklis P, Bauer C, Yin M, Vasioukhin V, Degenstein L, Fuchs E (1998) Desmoplakin is required early in development for assembly of desmosomes and cytoskeletal linkage. *J Cell Biol* **143:** 2009–2022

Ganguli-Indra G, Wasylyk C, Liang X, Millon R, Leid M, Wasylyk B, Abecassis J, Indra AK (2009) CTIP2 expression in human head and neck squamous cell carcinoma is linked to poorly differentiated tumor status. *PLoS One* **4:** e5367

Gao Z, Ure K, Ables JL, Lagace DC, Nave KA, Goebbels S, Eisch AJ, Hsieh J (2009) Neurod1 is essential for the survival and maturation of adult-born neurons. *Nat Neurosci* **12:** 1090–1092

Garrod D, Chidgey M (2008) Desmosome structure, composition and function. *Biochim Biophys Acta* **1778:** 572–587

Goebbels S, Bormuth I, Bode U, Hermanson O, Schwab MH, Nave KA (2006) Genetic targeting of principal neurons in neocortex and hippocampus of NEX-Cre mice. *Genesis* **44:** 611–621

Golonzhka O, Leid M, Indra G, Indra AK (2007) Expression of COUP-TF-interacting protein 2 (CTIP2) in mouse skin during development and in adulthood. *Gene Expr Patterns* **7:** 754–760

Golonzhka O, Liang X, Messaddeq N, Bornert JM, Campbell AL, Metzger D, Chambon P, Ganguli-Indra G, Leid M, Indra AK (2009) Dual role of COUP-TF-interacting protein 2 in epidermal homeostasis and permeability barrier formation. *J Invest Dermatol* **129:** 1459–1470

Gonzales RB, DeLeon Galvan CJ, Rangel YM, Claiborne BJ (2001) Distribution of thorny excrescences on CA3 pyramidal neurons in the rat hippocampus. *J Comp Neurol* **430:** 357–368

Gorski JA, Talley T, Qiu M, Puelles L, Rubenstein JL, Jones KR (2002) Cortical excitatory neurons and glia, but not GABAergic neurons, are produced in the Emx1-expressing lineage. *J Neurosci* **22:** 6309–6314

Hand R, Bortone D, Mattar P, Nguyen L, Heng JI, Guerrier S, Boutt E, Peters E, Barnes AP, Parras C, Schuurmans C, Guillemot F, Polleux F (2005) Phosphorylation of Neurogenin2 specifies the migration properties and the dendritic morphology of pyramidal neurons in the neocortex. *Neuron* **48:** 45–62

Heimrich B, Frotscher M (1991) Differentiation of dentate granule cells in slice cultures of rat hippocampus: a Golgi/electron microscopic study. *Brain Res* **538:** 263–268

Hodge RD, Kowalczyk TD, Wolf SA, Encinas JM, Rippey C, Enikolopov G, Kempermann G, Hevner RF (2008) Intermediate progenitors in adult hippocampal neurogenesis: Tbr2 expression and coordinate regulation of neuronal output. *J Neurosci* **28:** 3707–3717

Hoogenraad CC, Bradke F (2009) Control of neuronal polarity and plasticity–a renaissance for microtubules? *Trends Cell Biol* **19:** 669–676

John A, Brylka H, Wiegreffe C, Simon R, Liu P, Jüttner R, Crenshaw EB III, Luyten FP, Jenkins NA, Copeland NG, Birchmeier C, Britsch S (2012) Bcl11a is required for neuronal morphogenesis and sensory circuit formation in dorsal spinal cord development. *Development* **139:** 1801–1811

Karalay O, Doberauer K, Vadodaria KC, Knobloch M, Berti L, Miquelajauregui A, Schwark M, Jagasia R, Taketo MM, Tarabykin V, Lie DC, Jessberger S (2011) Prospero-related homeobox 1 gene (Prox1) is regulated by canonical Wnt signaling and has a stage-specific role in adult hippocampal neurogenesis. *Proc Natl Acad Sci USA* **108:** 5807–5812

Kempermann G, Jessberger S, Steiner B, Kronenberg G (2004) Milestones of neuronal development in the adult hippocampus. *Trends Neurosci* **27:** 447–452

Koeser J, Troyanovsky SM, Grund C, Franke WW (2003) De novo formation of desmosomes in cultured cells upon transfection of genes encoding specific desmosomal components. *Exp Cell Res* **285:** 114–130

Kuwabara T, Hsieh J, Muotri A, Yeo G, Warashina M, Lie DC, Moore L, Nakashima K, Asashima M, Gage FH (2009) Wnt-mediated activation of NeuroD1 and retro-elements during adult neurogenesis. *Nat Neurosci* **12:** 1097–1105

Lechler T, Fuchs E (2007) Desmoplakin: an unexpected regulator of microtubule organization in the epidermis. *J Cell Biol* **176:** 147–154

Leid M, Ishmael JE, Avram D, Shepherd D, Fraulob V, Dolle P (2004) CTIP1 and CTIP2 are differentially expressed during mouse embryogenesis. *Gene Expr Patterns* **4:** 733–739

Li G, Kataoka H, Coughlin SR, Pleasure SJ (2009) Identification of a transient subpial neurogenic zone in the developing dentate gyrus and its regulation by Cxcl12 and reelin signaling. *Development* **136:** 327–335

Li G, Pleasure SJ (2007) Genetic regulation of dentate gyrus morphogenesis. *Prog Brain Res* **163:** 143–152

Li P, Burke S, Wang J, Chen X, Ortiz M, Lee SC, Lu D, Campos L, Goulding D, Ng BL, Dougan G, Huntly B, Gottgens B, Jenkins NA, Copeland NG, Colucci F, Liu P (2010) Reprogramming of T cells to natural killer-like cells upon Bcl11b deletion. *Science* **329:** 85–89

Liang X, Bhattacharya S, Bajaj G, Guha G, Wang Z, Jang HS, Leid M, Indra AK, Ganguli-Indra G (2012) Delayed cutaneous wound healing and aberrant expression of hair follicle stem cell markers in mice selectively lacking ctip2 in epidermis. *PLoS One* **7:** e29999

Liu M, Pleasure SJ, Collins AE, Noebels JL, Naya FJ, Tsai MJ, Lowenstein DH (2000) Loss of BETA2/NeuroD leads to malformation of the dentate gyrus and epilepsy. *Proc Natl Acad Sci USA* **97:** 865–870

Liu P, Li P, Burke S (2010) Critical roles of Bcl11b in T-cell development and maintenance of T-cell identity. *Immunol Rev* **238:** 138–149

Livak KJ, Schmittgen TD (2001) Analysis of relative gene expression data using real-time quantitative PCR and the 2(-Delta Delta C(T)) Method. *Methods* **25:** 402–408

Marthiens V, Kazanis I, Moss L, Long K, Ffrench-Constant C (2010) Adhesion molecules in the stem cell niche—more than just staying in shape? *J Cell Sci* **123:** 1613–1622

Muramatsu R, Ikegaya Y, Matsuki N, Koyama R (2007) Neonatally born granule cells numerically dominate adult mice dentate gyrus. *Neuroscience* **148:** 593–598

Pleasure SJ, Collins AE, Lowenstein DH (2000) Unique expression patterns of cell fate molecules delineate sequential stages of dentate gyrus development. *J Neurosci* **20:** 6095–6105

Redmer T, Diecke S, Grigoryan T, Quiroga-Negreira A, Birchmeier W, Besser D (2011) E-cadherin is crucial for embryonic stem cell pluripotency and can replace OCT4 during somatic cell reprogramming. *EMBO Rep* **12:** 720–726

Schwegler H, Crusio WE (1995) Correlations between radial-maze learning and structural variations of septum and hippocampus in rodents. *Behav Brain Res* **67:** 29–41

Schwegler H, Crusio WE, Brust I (1990) Hippocampal mossy fibers and radial-maze learning in the mouse: a correlation with spatial working memory but not with non-spatial reference memory. *Neuroscience* **34:** 293–298

Schwegler H, Lipp HP (1983) Hereditary covariations of neuronal circuitry and behavior: correlations between the proportions of hippocampal synaptic fields in the regio inferior and two-way avoidance in mice and rats. *Behav Brain Res* **7:** 1–38

Seuntjens E, Nityanandam A, Miquelajauregui A, Debruyn J, Stryjewska A, Goebbels S, Nave KA, Huylebroeck D, Tarabykin V (2009) Sip1 regulates sequential fate decisions by feedback signaling from postmitotic neurons to progenitors. *Nat Neurosci* **12:** 1373–1380

Topark-Ngarm A, Golonzhka O, Peterson VJ, Barrett Jr. B, Martinez B, Crofoot K, Filtz TM, Leid M (2006) CTIP2 associates with the NuRD complex on the promoter of p57KIP2, a newly identified CTIP2 target gene. *J Biol Chem* **281:** 32272–32283

Vasioukhin V, Bowers E, Bauer C, Degenstein L, Fuchs E (2001) Desmoplakin is essential in epidermal sheet formation. *Nat Cell Biol* **3:** 1076–1085

Wakabayashi Y, Watanabe H, Inoue J, Takeda N, Sakata J, Mishima Y, Hitomi J, Yamamoto T, Utsuyama M, Niwa O, Aizawa S, Kominami R (2003) Bcl11b is required for differentiation and survival of alphabeta T lymphocytes. *Nat Immunol* **4:** 533–539

Yan Y, Frisen J, Lee MH, Massague J, Barbacid M (1997) Ablation of the CDK inhibitor p57Kip2 results in increased apoptosis and delayed differentiation during mouse development. *Genes Dev* **11:** 973–983

Yilmazer-Hanke DM, Wigger A, Linke R, Landgraf R, Schwegler H (2004) Two Wistar rat lines selectively bred for anxiety-related behavior show opposite reactions in elevated plus maze and fear-sensitized acoustic startle tests. *Behav Genet* **34:** 309–318

Zhao C, Deng W, Gage FH (2008) Mechanisms and functional implications of adult neurogenesis. *Cell* **132:** 645–660